# Temperature- and Rate-Dependent Pathways in Formation of Metastable Silicon Phases under Rapid Decompression

Chuanlong Lin,[1,*] Xuqiang Liu,[1] Dongliang Yang,[2] Xiaodong Li,[2] Jesse S. Smith,[3] Bihan Wang,[1] Haini Dong,[1] Shourui Li,[4] Wenge Yang,[1] and John S. Tse[1,5]

[1]*Center for High Pressure Science and Technology Advanced Research, Beijing 100094, People's Republic of China*
[2]*Beijing Synchrotron Radiation Facility, Institute of High Energy Physics, Chinese Academy of Science, Beijing 100049, China*
[3]*High Pressure Collaborative Access Team, X-ray Science Division, Argonne National Laboratory, Argonne, Illinois 60439, USA*
[4]*Institute of Fluid Physics, CAEP, Mianyang 621900, China*
[5]*Department of Physics and Engineering Physics, University of Saskatchewan, Saskatoon, Saskatchewan S7N 5E2, Canada*

(Received 19 May 2020; revised 27 July 2020; accepted 15 September 2020; published 7 October 2020)

High-pressure metallic $\beta$-Sn silicon (Si-II), depending on temperature, decompression rate, stress, etc., may transform to diverse metastable forms with promising semiconducting properties under decompression. However, the underlying mechanisms governing the different transformation paths are not well understood. Here, two distinctive pathways, viz., a thermally activated crystal-crystal transition and a mechanically driven amorphization, were characterized under rapid decompression of Si-II at various temperatures using *in situ* time-resolved x-ray diffraction. Under slow decompression, Si-II transforms to a crystalline bc8/r8 phase in the pressure range of 4.3–9.2 GPa through a thermally activated process where the overdepressurization and the onset transition strain are strongly dependent on decompression rate and temperature. In comparison, Si-II collapses structurally to an amorphous form at around 4.3 GPa when the volume expansion approaches a critical strain via rapid decompression beyond a threshold rate. The occurrence of the critical strain indicates a limit of the structural metastability of Si-II, which separates the thermally activated and mechanically driven transition processes. The results show the coupled effect of decompression rate, activation barrier, and thermal energy on the adopted transformation paths, providing atomistic insight into the competition between equilibrium and nonequilibrium pathways and the resulting metastable phases.

DOI: 10.1103/PhysRevLett.125.155702

Silicon displays diverse allotropes at ambient conditions and has been the focus of a wealth of fundamental and applied research [1–8]. The metastable forms, such as the bc8, r8, and amorphous Si ($a$-Si), as promising semiconductor phases have attracted increased attention because of the wide range band gap properties [9–16]. They can be synthesized from high-pressure metallic $\beta$-Sn Si (Si-II) via decompression [7–10,17–20]. However, previous studies have shown the transformation mechanism and kinetic pathways for Si-II are strongly affected by temperature, decompression rate (unloading rate), shear stress, sample size, etc. [3,8,11,18,21–29]. For example, Si-II amorphizes under static decompression at temperatures below 120 K, whereas it transforms to metastable crystalline bc8/r8 Si at room temperature [3,17]. Indentation experiments at room temperature show time-dependent transition pathways, in which Si-II transforms to the bc8/r8 phase under slow decompression, but to $a$-Si under rapid decompression [23,28–30]. The time-dependent, multiple kinetic transition pathways have also been reported on the millisecond timescale in diamond anvil cell experiments [18,21]. The question arises about how these thermophysical factors (temperature, decompression rate, pressure) are coupled together to affect the kinetic pathways and the atomistic mechanism. The fundamental knowledge of the structural evolution of high-pressure metallic $\beta$-Sn Si toward the promising semiconductor phases is rather scarce.

To exploit the unique properties of materials for practical use, it is essential to control the synthesis of the desirable metastable phases. Thus, a fundamental understanding on the formation conditions, such as temperature, pressure, and (de)compression rate, is critical. Earlier studies with intermediate timescale between static compression and shock wave experiments have shown that the coupling of temperature and (de)compression rate has a significant influence on the transformation processes and kinetic pathways under rapid compression [21,31–34]. For example, in thermally activated transformation of ice ($H_2O$) and KCl, the onset transition pressures (i.e., overpressurization) were found to change with compression rate and temperature [33,34]. The transformation pathways in ice at low $T$ were observed to be strongly dependent on temperature and (de)compression rate [31,32,35]. Unlike static and shock-induced transformation in which the activation barrier, related to the rearrangement of atomic bonds, is given less consideration or neglected, the end products are the results of the complex interplay between (de)compression rate, temperature, and intrinsic activation barrier [31,32]. It was

 

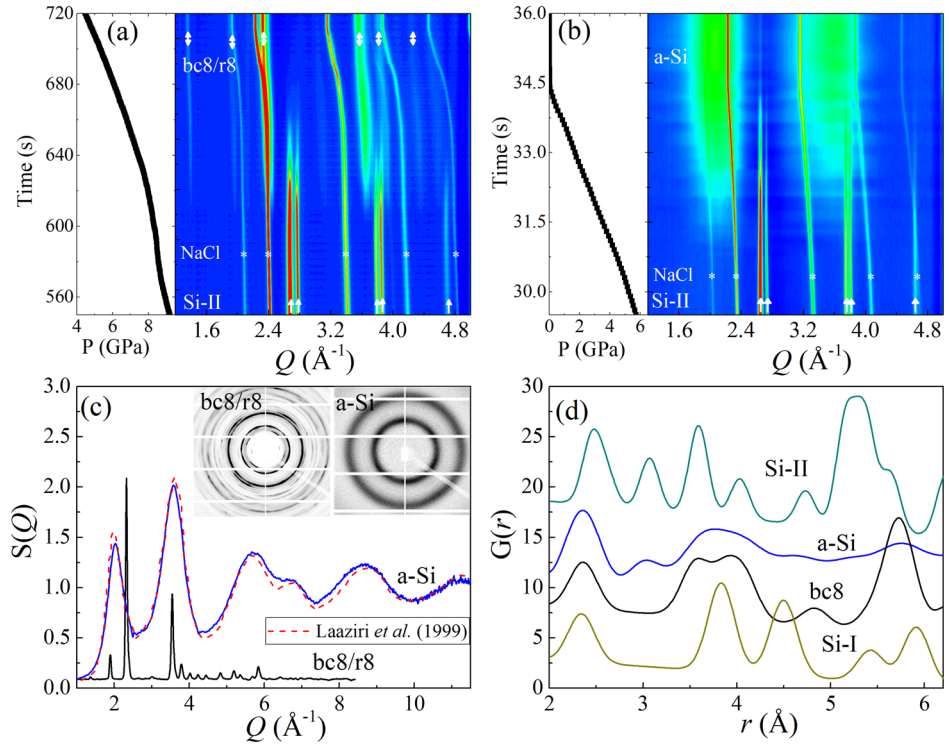


FIG. 1. Rate dependence of kinetic pathways in the structural evolution of Si-II under decompression with different rate. The background was subtracted for the typical integrated x-ray diffraction patterns. (a) Slow decompression (~0.024 GPa/s) of Si-II leads to the formation of bc8/r8 Si at 260 K. The Bragg peaks of NaCl, used as pressure marker and transmitting medium, are marked with asterisks. Si-II and bc8/r8 phases are indicated by up arrows and up-down arrows, respectively. (b) Under rapid decompression (~1.22 GPa/s) at 260 K, Si-II transforms to amorphous Si. (c) Structure factor for amorphous Si obtained by transformation of Si-II under rapid decompression at room temperature. The diffraction pattern of the crystalline bc8/r8 phase is shown for comparison. The insets are the raw x-ray diffraction images of *a*-Si and the bc8/r8 phase. Red dashed line shows the structure factor of as-implanted amorphous Si for comparison [44]. (d) The reduced pair distribution function of amorphous Si obtained by Fourier transform from the structure factor of (c). The calculated reduced pair distribution functions of the crystalline Si-I, bc8, and Si-II are shown for comparison.

found that there is a threshold (de)compression rate, which separates transition processes and exhibits an approximately exponential relationship with inverse temperature and kinetic energy barrier. Similarly in Si, multiple transition paths, governed by temperature and rate, have also been reported in the decompression of Si-II, which led to different end structures [3,21]. So far, there is no quantitative description or theoretical model to elucidate the relationship among the external loading rate, temperature, and energy barrier. In this Letter, we present detailed investigation of the structural evolution of Si-II toward the metastable Si under decompression using *in situ* time-resolved x-ray diffraction and study the coupled effect of temperature and decompression rate on the thermally activated crystal-crystal transformation and mechanically driven amorphization.

The experimental detail in the present Letter is similar to that described in previous studies [31,32] and can be found in the Supplemental Material [36]. High-pressure metallic Si-II was prepared by compressing the Si sample with the diamond cubic structure (Si-I) up to ~12 GPa at a given temperature. Figures 1(a) and 1(b) show the comparison of kinetic pathways in structural evolution of Si-II under decompression with different rates below the equilibrium phase boundary where Gibbs free energies between Si-I and Si-II are equal. Under slow decompression (~0.024 GPa/s) at 260 K, Si-II transforms gradually to a crystalline phase at ~8.8 GPa and coexists in the pressure range of 5.0–8.8 GPa [Fig. 1(a)]. The structure of the crystalline phase is indexed as the r8 phase and transforms successively to bc8 Si under further decompression. These observations are consistent with previous reports [1]. We denote the crystalline Si transformed from Si-II as the bc8/r8 phase, as both structures are very close and coexist at ambient pressure and low temperature. Under rapid decompression with a relatively higher rate (~1.22 GPa/s), Si-II is overdepressurized down to ~4.0 GPa where it starts to amorphize with the appearance of two characteristic diffraction halo peaks at ~2.02 and 3.58 $Å^{-1}$ [Fig. 1(b)]. Under further decompression to ambient pressure, the relative intensity of the amorphous Si phase increases with a concomitant decrease in the intensities of the Bragg reflections of Si-II. A small amount of Si-II remains and coexists with *a*-Si even at ambient pressure [Fig. 1(b)]. At a

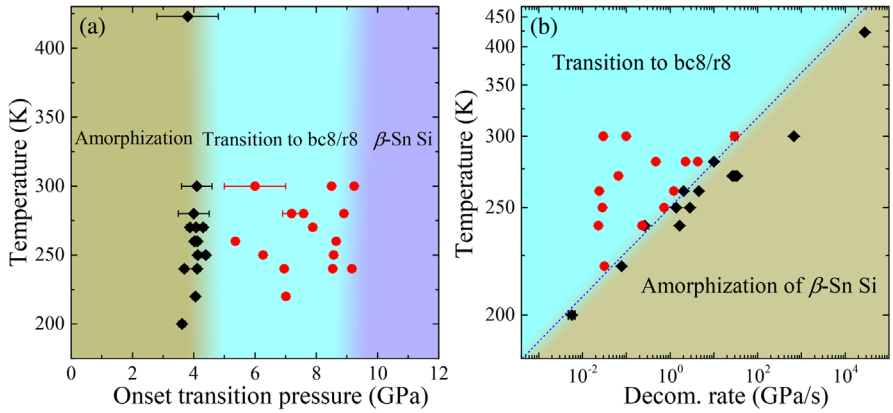


FIG. 2. Experimental summary of the phase transformations of $\beta$-Sn Si under decompression at different temperatures. (a) The onset transition pressures at different temperatures. Red solid circles and black solid diamonds indicate the onset transition pressures from $\beta$-tin Si to bc8/r8 and to $a$-Si at different decompression rates, respectively. The onset transition pressures of the $\beta$-Sn to bc8/r8 transition, varying from ~9.2 to ~5 GPa, correspond to the different decompression rates. The amorphization occurs at around 4.3 GPa, showing weak temperature and decompression-rate dependence. (b) Observed metastable phases at various decompression rates and different temperatures. Red symbols represent the bc8/r8 phase, while black symbols indicate $a$-Si.

moderate decompression rate, Si-II was observed to transform to a mixture of bc8/r8 and $a$-Si (Fig. S1).

Different pressure media (He, Ne, NaCl, no pressure medium) have been used to investigate the stress effect on the transition sequence of Si-II. In the gas medium (He or Ne), which provided hydrostatic conditions, the same rate-dependent kinetic pathways were observed as compared to the results using NaCl as pressure transmitting medium at room temperature (Fig. S1). This observation indicates that the intrinsic transition processes on the decompression of Si-II have not changed at the quasihydrostatic and hydrostatic conditions and thus rules out the possibility of stress effect on the rate-dependent transition pathways in the pressure medium of NaCl. At nonhydrostatic conditions (i.e., without a pressure transmitting medium), the transition sequence of Si-II and the recovered sample was inhomogeneous. In this case, the metastable phases formed not only include amorphous Si and the bc8/r8 phase, but also some other metastable crystalline phases (see more details in Supplemental Material [36] and Fig. S2).

Figures 1(c) and 1(d) compare the structures of the product phases transformed from Si-II. $a$-Si shows a homogeneous pattern with broad diffraction peaks, while the bc8/r8 phase shows characteristic texture and orientation-dependent patterns with sharp Bragg peaks [inset of Fig. 1(c)]. It should be noted that $a$-Si is not the nanocrystalline form of the observed crystalline phases (e.g., Si-I, bc8/r8, or Si-II). This is because there is a clear difference in peak positions of x-ray diffraction patterns between the $a$-Si and nanocrystalline Si. Furthermore, broadening of the nanocrystalline diffraction peaks to mimic the effect of small grain sizes does not match well with the observed amorphous pattern. On the other hand, the structure factor of $a$-Si shows similarities in peak positions and widths to that of as-implanted amorphous Si prepared by MeV Si implantation [Fig. 1(c)] [44]. Assuming the density is the same as implanted amorphous Si, the mean nearest-neighbor coordination bond distance and coordination number for $a$-Si are calculated from the reduced pair distribution $[G(r)]$ to be ~2.35 Å and ~4.2, respectively, close to ~2.36 Å and 4 for bc8 phase, ~2.34 Å and 4 for Si-I, but smaller than ~2.48 Å and 6 for the remnant $\beta$-Sn Si [Fig. 1(d)]. These suggest a similar local environment with approximate tetrahedral coordination in $a$-Si. A weak peak is observed at 3.02 Å in the $[G(r)]$ of $a$-Si, which is absent in bc8/r8. This feature may be associated with the second nearest-neighbor distance in Si-II at 3.07 Å [Fig. 1(d)]. It implies that $a$-Si may be still compacted and inherits the structural feature of the parent Si-II.

The structural difference between the $a$-Si and bc8/r8 phases results in distinctively different thermal stability and phase transformation sequences. Heating amorphous Si at ambient pressure led to the crystallization into Si-I (Fig. S3), instead of transforming to a hexagonal structure as reported in the bc8/r8 phase [7]. We also compressed amorphous Si up to ~12 GPa and observed transformation to the r8 phase at around 9 GPa, followed by the r8 to Si-II transition (Fig. S4). These experimental results raise a question regarding the nature of the kinetic processes in which Si-II transforms to the metastable product phases with different morphology and thermal stability.

To resolve the puzzle, we investigated the rate-dependent transition pathways of Si-II at temperatures of 200, 220, 240, 250, 270, 280, 300, and 423 K (Figs. S5–S9). Figure 2(a) summarizes the onset transition pressures ($P_0$) under decompression of Si-II at various temperatures. Two distinct pressure regions are clearly revealed, viz., the phase transformation of Si-II to the crystalline bc8/r8 phase in the pressure range of ~4.3–9.2 GPa and $a$-Si below 4.3 GPa. In the pressure range of 4.3–9.2 GPa, the onset transition

pressure for the Si-II to bc8/r8 transition strongly depends on the decompression rate and temperature. The higher decompression rates will lead to higher overdepressurization (Fig. S10). Interestingly, Si-II collapses structurally into $a$-Si when it is decompressed to a critical pressure point of ~4.3 GPa, ~5 GPa beyond the thermal equilibrium region of Si-II. The critical pressure for amorphization is independent of decompression rate and temperature, indicating a limit of the structural metastability of $\beta$-Sn Si.

Figure 2(b) summarizes the experimental results of the observed bc8/r8 and $a$-Si transformed from Si-II at different decompression rates and temperatures. The diagram shows a boundary separating the Si-II to bc8/r8 transition and amorphization [blue dashed line in Fig. 2(b)]. Close to the boundary, a mixture of bc8/r8 and $a$-Si coexists (Fig. S1). The boundary indicates existence of a threshold decompression rate ($\beta_c$) at given temperature, namely, below which Si-II transforms to the bc8/r8 phase and above which rapid decompression leads to the formation of $a$-Si. When Fig. 2(b) is plotted with log of decompression rate and inverse temperature, the boundary shows an approximately linear relationship between $\beta_c$ and $T$, i.e., there is an Arrhenius relationship between the threshold rate and temperature with $\beta_c = C_0 \exp(-Q/k_B T)$ [32,45,46], where $C_0$ is a constant with units of GPa/s and $Q$ is the thermal activation energy. Fitting the experimental data yields $C_0$ of $2.0 \times 10^9$ GPa/s and $Q$ of 44(2) kJ/mol. It should be noted that the threshold rate corresponds to the critical transition pressure of ~4.3 GPa in Fig. 2(a) and is the minimum decompression rate required to bypass the phase transformation from Si-II to bc8/r8 phase. Above 4.3 GPa, the crystalline phase transformed by overdepressurization of Si-II is the result of competition among the external decompression rate, temperature, and energy barrier. This is the characteristic feature of thermally activated mechanism for Si-II to bc8/r8 transition. In contrast, amorphization of Si-II shows temperature and rate independence and is an athermal process. It is driven by a structural instability, i.e., the mechanical instability.

Figure 3 shows the structural evolution of Si-II along the transition to the bc8/r8 phase (red symbols) and $a$-Si (black symbols) under decompression at 260 K. In the thermally activated crystal-crystal transition region, the crystal axes $a$ and $b$, and atomic volume of $\beta$-Sn Si, increase with reduced pressure. There is no anomaly in the lattice parameters near the onset transition pressure of the phase transformation to the bc8/r8 phase. In comparison, preceding the amorphization at ~5 GPa, the variation of the lattice parameter $a$ of Si-II is rather flat and even decreases at lower pressures, while the lattice parameter $c$ expands with the decrease of pressure. The anisotropic expansion of the tetragonal structure is clearly displayed in the ratio of $a/c$ (Fig. 3). This indicates a shear distortion along the basal $ab$ plane in the tetragonal structure of Si-II, a phenomenon similar to

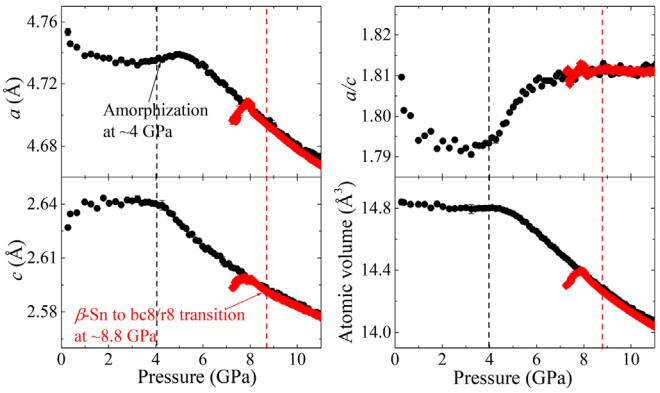


FIG. 3. Lattice evolution of $\beta$-Sn Si under decompression at 260 K. Black and red solid circles represent the amorphization and Si-II to bc8/r8 transition, respectively. Black and red dashed lines indicate the onset transition pressures.

the pressure-induced amorphization of hexagonal crystalline ice at low $T$ [47,48], and implies an elastic instability prior to amorphization. It should be noted that Si-II coexists with $a$-Si below 4.3 GPa, which may be due to the stress effect between particle grains of the product and parent phases. Remarkably, the unit cell volume of Si-II is almost constant under decompression from ~4.3 GPa to ambient pressure. The trend persists at other temperatures and different decompression rates (see Fig. S11). This implies a limit of the structural metastability of Si-II beyond the equilibrium phase boundary, at which the structure collapses mechanically without the aid of thermal fluctuations.

To quantify the relationship among temperature, decompression rate, and volume, the onset transition strain is defined by $\varepsilon = (V_0 - V_{tr})/V_{tr}$, where $V_{tr}$ and $V_0$ are the volumes of Si-II at the thermal equilibrium pressure ($P_{tr}$) and $P_0$, respectively. Figure 4(a) summarizes the onset transition strain as a function of overdepressurization ($\Delta P = P_{tr} - P_0$) at different temperatures and decompression rates. In the thermally activated transition, $\varepsilon$ increases with overdepressurization until it approaches a critical value of ~0.043. It seems that the Si-II has a strain limit in the expansion of the volume beyond the equilibrium boundary. The critical strain of Si-II corresponds to the limit of the structural metastability.

Figure 4(b) shows a plot of the onset transition strain of Si-II as a function of temperature at given decompression rates ($\beta$). Previous studies have indicated that the thermally activated transformation generally follows the transition state theory that can describe combined effect of temperature and decompression rate (or strain rate) on the transition strain and stress [49–52]. The onset transition strain (or overdepressurization) is a result of the competition between thermal activation rate and external strain rate ($\dot{\varepsilon}$). At given strain rate, the onset transition strain is equal to $\dot{\varepsilon}\Delta t$ with $\dot{\varepsilon} = (d\varepsilon/dt) = (dV/V_0 dP)(dP/dt)$, where $\Delta t$ is the decompression time required to bypass the overpressure range, and $dP/dt$ is the decompression rate. At $P_0$,

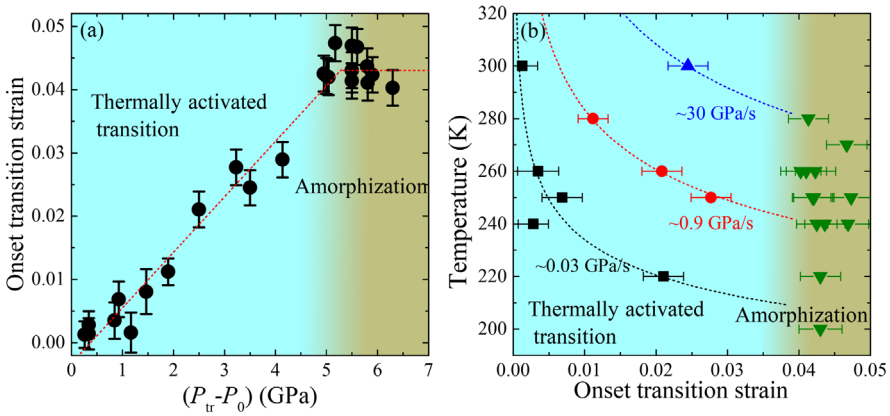


FIG. 4. Illustration of onset transition strain as a function of (a) overdepressurization at all decompression rates and temperatures and (b) temperature at different decompression rates. The red dashed line in (a) is a guide to the eye. The experimental data are used in (b) when the decompression rates are close. $P_{tr}$ with value of 9.5 GPa is extracted according to the phase boundary of Fig. 2(a) and is referred to the static data [2,5]. Black and red dashed lines are fitting lines. The blue dashed line is calculated as a guide to the eye.

the structural transformation occurs when the thermal activation rate is comparable to the decompression rate. Here, $1/\Delta t$ is assumed to be proportional to thermal activation rate determined by the Arrhenius equation, i.e., rate $\sim \exp(-Q_{\mathrm{eff}}/RT)$, where $Q_{\mathrm{eff}}$ is effective activation energy in the overpressure range [49–51]. $\dot{\varepsilon}$ is approximately constant at given decompression rate as $dV/V_0 dP$ changes slightly with pressure in the thermal activation region. Thus, we obtain $\varepsilon = C_0(\beta) \cdot \exp(Q_{\mathrm{eff}}/RT)$ to approximately describe the $\varepsilon$-$T$ relationship at a given rate, where $C_0$ is a decompression-rate-dependent constant.

Fitting the experimental data yields $Q_{\mathrm{eff}} = 22(1)$ kJ/mol with $C_0 = 1.23 \times 10^{-7}$ at ~0.03 GPa/s, and $Q_{\mathrm{eff}} = 18(1)$ kJ/mol with $C_0 = 5.60 \times 10^{-6}$ at ~0.9 GPa/s [Fig. 4(b)]. It should be noted that $Q_{\mathrm{eff}}$ is an average order of magnitude as it describes the entire decompression process. The higher decompression rate leads to higher overdepressurization with low $Q_{\mathrm{eff}}$. The fitted activation energy is close to the calculated enthalpy barrier of ~15 kJ/mol for the transformation of Si-II toward the bc8 phase at 8 GPa [53], which is the kinetic barrier in the local-bond-twisting reconstruction process and decreases with reduced pressure. The kinetic barrier is indicated to play a central role in selecting the decompression pathway in the thermally activated crystal-crystal transitions [53]. Under hydrostatic conditions, the barrier for phase transformation from Si-II to bc8 is calculated to be lower than those of the transformation to the tetragonal ST12 and to Si-I [53,54], which is consistent with the experimental observations of the Si-II to bc8/r8 transition.

The relationship among the onset transition strain, temperature, and decompression rate shows that in the thermally activated transition region $\varepsilon$ increases monotonically as the temperature decreases at given decompression rate. At a given temperature, the onset transition pressure and strain increase as the decompression rate increases. However, the structure of Si-II cannot expand indefinitely and will reach a critical strain at the threshold rate, i.e., the limit of the structural metastability. At the critical strain, the $\varepsilon$-$T$ relationship is interrupted by the amorphization [Fig. 4(b)]. The transformation mechanism in Si-II changes from a thermal activation process to a temperature-independent process (athermal process) driven by mechanical instability. The critical strain can be approached via rapid decompression at high temperature or slow decompression at low temperature, where the mechanical instability leads to the amorphization. This explains the previous observations in the formation of $a$-Si under the decompression of Si-II [3,17,21].

The above transition mechanism governing the transformation paths in Si-II may be ubiquitous. It can be used to interpret temperature- and rate-dependent kinetic pathways and pressure-induced amorphization in other materials, such as ice. Previous studies show the temperature- and rate-dependent formation of amorphous ice in crystalline ice I or ice VII, bypassing thermally driven crystalline-crystalline transition under rapid compression (or decompression) [31,32]. The threshold rate, separating the thermally driven crystal-crystal transition and amorphization, has an exponential relationship with temperature and kinetic barrier. These behaviors are similar to the transformation of Si-II, indicating the analogous underlying mechanism in both Si-II and crystalline ice. Therefore, the (de)compression rate and temperature mainly affect the thermally activated crystal-crystal transition in ice with a significant influence on the transition pressure and strain. When the critical strain is approached, the parent crystalline ice reaches the limit of the structural metastability and exhibits mechanical instability, where amorphization occurs. On the other hand, we should note that the kinetic processes in the formation of amorphous phases are different between Si-II and crystalline ice, as the kinetic barrier for the former derives from the hindrance in the formation

of covalent bond from the metallic bond of Si-II and, for the latter, is due to the reorientation of the hydrogen-bond network. The structure of the crystalline ice shows the elastic instability with softening of the elastic modulus and violation of Born criteria prior to the amorphization [47]. Whether this occurs in Si-II should be further confirmed.

In summary, we reveal two distinct kinetic pathways of $\beta$-Sn Si, viz., a thermally activated transition and a mechanically driven amorphization, under rapid decompression using time-resolved x-ray diffraction. The present results show the coupled effect of the decompression rate, temperature, and kinetic barrier on the transition pathways, providing deep insight into the fundamental understanding on the formation of metastable silicon phases. This is of fundamental significance in controlled synthesis of the desirable metastable phases for practical use.

The authors thank Saori Kawaguchi, Curtis Kenney-Benson, and Richard Ferry for technical support and like to thank National Nature Science Foundation of China (No. 11974033, No. 51527801, and No. U1930401), the Science Challenge Project No. TZ2016001, and the Foundation of National Key Laboratory of Shockwave and Detonation Physics of China (No. 6142A03191002 and No. 6142A0306010817). *In situ* high-pressure, low-temperature x-ray diffraction measurements were conducted at sector 16 ID-B, HPCAT of Advanced Photon Source, which are supported by DOE-NNSA under Award No. DE-NA0001974, with partial instrumentation funding by NSF. Advanced Photon Source is supported by DOE-BES, under Award No. DE-AC02-06CH11357 by UChicago Argonne, LLC. The partial synchrotron radiation experiments were performed at the 4W2 beamline of BSRF and at BL10XU under the approval of the Japan Synchrotron Radiation Research Institute (JASRI) (Proposals No. 2019B1059, No. 2019B4267, and No. 2019A4273).

C. Lin and X. Liu contributed equally to this work.

*chuanlong.lin@hpstar.ac.cn

[1] R. H. Wentorf and J. S. Kasper, Science **139**, 338 (1963).
[2] R. O. Piltz, J. R. Maclean, S. J. Clark, G. J. Ackland, P. D. Hatton, and J. Crain, Phys. Rev. B **52**, 4072 (1995).
[3] M. Imai, T. Mitamura, K. Yaoita, and K. Tsuji, High Press. Res. **15**, 167 (1996).
[4] M. Gamero-Castaño, A. Torrents, L. Valdevit, and J.-G. Zheng, Phys. Rev. Lett. **105**, 145701 (2010).
[5] J. Crain, G. J. Ackland, J. R. Maclean, R. O. Piltz, P. D. Hatton, and G. S. Pawley, Phys. Rev. B **50**, 13043 (1994).
[6] L. Rapp, B. Haberl, C. J. Pickard, J. E. Bradby, E. G. Gamaly, J. S. Williams, and A. V. Rode, Nat. Commun. **6**, 7555 (2015).
[7] B. Haberl, M. Guthrie, S. V. Sinogeikin, G. Shen, J. S. Williams, and J. E. Bradby, High Press. Res. **35**, 99 (2015).
[8] B. Haberl, T. A. Strobel, and J. E. Bradby, Appl. Phys. Rev. **3**, 040808 (2016).
[9] H. Zhang, H. Liu, K. Wei, O. O. Kurakevych, Y. Le Godec, Z. Liu, J. Martin, M. Guerrette, G. S. Nolas, and T. A. Strobel, Phys. Rev. Lett. **118**, 146601 (2017).
[10] S. Wong, B. Haberl, B. C. Johnson, A. Mujica, M. Guthrie, J. C. McCallum, J. S. Williams, and J. E. Bradby, Phys. Rev. Lett. **122**, 105701 (2019).
[11] S. Ruffell, K. Sears, A. P. Knights, J. E. Bradby, and J. S. Williams, Phys. Rev. B **83**, 075316(R) (2011).
[12] B. D. Malone, J. D. Sau, and M. L. Cohen, Phys. Rev. B **78**, 161202(R) (2008).
[13] B. D. Malone, J. D. Sau, and M. L. Cohen, Phys. Rev. B **78**, 035210 (2008).
[14] M. Kondo, T. Matsui, Y. Nasuno, H. Sonobe, and S. Shimizu, Thin Solid Films **501**, 243 (2006).
[15] H. Gleskova and S. Wagner, IEEE Electron Device Lett. **20**, 473 (1999).
[16] P. Servati, S. Prakash, A. Nathan, C. Py, and J. Vacuum Sci. Technol. A **20**, 1374 (2002).
[17] V. V. Brazhkin, A. G. Lyapin, S. V. Popova, and R. N. Voloshin, Phys. Rev. B **51**, 7549 (1995).
[18] Y.-X. Zhao, F. Buehler, J. R. Sites, and I. L. Spain, Solid State Commun. **59**, 679 (1986).
[19] D. R. Clarke, M. C. Kroll, P. D. Kirchner, R. F. Cook, and B. J. Hockey, Phys. Rev. Lett. **60**, 2156 (1988).
[20] A. Mujica, A. Rubio, A. Muñoz, and R. J. Needs, Rev. Mod. Phys. **75**, 863 (2003).
[21] J. S. Smith, S. V. Sinogeikin, C. Lin, E. Rod, L. Bai, and G. Shen, Rev. Sci. Instrum. **86**, 072208 (2015).
[22] D. Ge, V. Domnich, and Y. Gogotsi, J. Appl. Phys. **95**, 2725 (2004).
[23] V. Domnich, Y. Gogotsi, and S. Dub, Appl. Phys. Lett. **76**, 2214 (2000).
[24] E. R. Weppelmann, J. S. Field, and M. V. Swain, J. Mater. Res. **8**, 830 (1993).
[25] I. Zarudi, L. C. Zhang, W. C. D. Cheong, and T. X. Yu, Acta Mater. **53**, 4795 (2005).
[26] I. Zarudi, J. Zou, and L. C. Zhang, Appl. Phys. Lett. **82**, 874 (2003).
[27] J. E. Bradby, J. S. Williams, J. Wong-Leung, M. V. Swain, and P. Munroe, Appl. Phys. Lett. **77**, 3749 (2000).
[28] A. Kailer, K. G. Nickel, and Y. G. Gogotsi, J. Raman Spectrosc. **30**, 939 (1999).
[29] S. Ruffell, J. E. Bradby, J. S. Williams, and P. Munroe, J. Appl. Phys. **102**, 063521 (2007).
[30] C. R. Das, S. Dhara, Y.-R. Jeng, P.-C. Tsai, H. C. Hsu, B. Raj, A. K. Bhaduri, S. K. Albert, A. K. Tyagi, L. C. Chen, and K. H. Chen, Appl. Phys. Lett. **96**, 253113 (2010).
[31] C. Lin, J. S. Smith, S. V. Sinogeikin, and G. Shen, Proc. Natl. Acad. Sci. U.S.A. **115**, 2010 (2018).
[32] C. Lin, J. S. Smith, X. Liu, J. S. Tse, and W. Yang, Phys. Rev. Lett. **121**, 225703 (2018).
[33] C. Lin, J. S. Smith, S. V. Sinogeikin, C. Park, Y. Kono, C. Kenney-Benson, E. Rod, and G. Shen, J. Appl. Phys. **119**, 045902 (2016).
[34] M. Bauer, M. S. Elsaesser, K. Winkel, E. Mayer, and T. Loerting, Phys. Rev. B **77**, 220105(R) (2008).
[35] C. A. Tulk, J. J. Molaison, A. R. Makhluf, C. E. Manning, and D. D. Klug, Nature (London) **569**, 542 (2019).

[36] See Supplemental Material at http://link.aps.org/supplemental/10.1103/PhysRevLett.125.155702 for experimental details and additional x-ray diffraction results at various temperatures, which includes Refs. [21, 37–43].
[37] R. Hrubiak, S. Sinogeikin, E. Rod, and G. Shen, Rev. Sci. Instrum. **86**, 072202 (2015).
[38] F. Birch, J. Geophys. Res. **91**, 4949 (1986).
[39] H. K. Mao, J. Xu, and P. M. Bell, J. Geophys. Res. **91**, 4673 (1986).
[40] S. V. Sinogeikin, J. S. Smith, E. Rod, C. Lin, C. Kenney-Benson, and G. Shen, Rev. Sci. Instrum. **86**, 072209 (2015).
[41] J. Liu, Chin. Phys. B **25**, 076106 (2016).
[42] N. Hirao, S. I. Kawaguchi, K. Hirose, K. Shimizu, E. Ohtani, and Y. Ohishi, Matter Radiat. Extremes **5**, 018403 (2020).
[43] C. Prescher and V. B. Prakapenka, High Press. Res. **35**, 223 (2015).
[44] K. Laaziri, S. Kycia, S. Roorda, M. Chicoine, J. L. Robertson, J. Wang, and S. C. Moss, Phys. Rev. B **60**, 13520 (1999).
[45] A. K. Singh, Mater. Sci. Forum **3**, 291 (1985).
[46] S. Glasstone, K. J. Laidler, and H. Eyring, *The Theory of Rate Processes* (McGraw-Hill, New York, 1941).
[47] J. S. Tse, J. Chem. Phys. **96**, 5482 (1992).
[48] C. Lin, X. Yong, J. S. Tse, J. S. Smith, S. V. Sinogeikin, C. Kenney-Benson, and G. Shen, Phys. Rev. Lett. **119**, 135701 (2017).
[49] Z. Bai and Y. Fan, Phys. Rev. Lett. **120**, 125504 (2018).
[50] Y. Fan, Y. N. Osetsky, S. Yip, and B. Yildiz, Phys. Rev. Lett. **109**, 135503 (2012).
[51] T. Zhu, J. Li, A. Samanta, A. Leach, and K. Gall, Phys. Rev. Lett. **100**, 025502 (2008).
[52] Y. Fan, Y. N. Osetskiy, S. Yip, and B. Yildiz, Proc. the Natl. Acad. Sci. U.S.A. **110**, 17756 (2013).
[53] J.-T. Wang, C. Chen, H. Mizuseki, and Y. Kawazoe, Phys. Rev. Lett. **110**, 165503 (2013).
[54] L. Zhu, R. E. Cohen, and T. A. Strobel, J. Phys. Chem. Lett. **10**, 5019 (2019).